Mansoura Engineering Journal

Volume 38 | Issue 3 Article 13

8-11-2020

Simulation of Water Hammer in Viscoelastic Pipes.

Hassan Mansour
Mechanical Power Engineering Department, Faculty of Engineering, Mansoura University, Mansoura, Egypt

M. Mohamed
Mechanical Power Engineering Department, Faculty of Engineering, Mansoura University, Mansoura, Egypt, msafwat@mans.edu.eg

Berge Djebedjian
Mechanical Power Engineering Department, Faculty of Engineering, Mansoura University, El-Mansoura 35516, Egypt, bergedje@mans.edu.eg

Mohamed Tawfik
Mechanical Power Engineering Department, Faculty of Engineering, Mansoura University, Mansoura, Egypt, m.m.h.tawfik@mans.edu.eg

SIMULATION OF WATER HAMMER IN VISCOELASTIC PIPES

محاكاة ظاهرة الطرق المائي في أنابيب مصنوعة من المواد البلاستيكية

Hassan Mansour, Mohamed Safwat, Berge Djebedjian, and Mohamed Tawfik

Mechanical Power Engineering Department, Faculty of Engineering,
Mansoura University, El-Mansoura 35516, Egypt
Emails: mhsaadanyh@yahoo.com, msafwat@mans.edu.eg, bergedje@mans.edu.eg,
m.m.h.tawfik@mans.edu.eg

الخلاصة:

إن السلوك الميكانيكي لمادة الأنبوب يؤثر على شكل التذبذب في الضغط أثناء حدوث ظاهرة الطرق المائي ؛ حيث وجد أنه في حالة الأنابيب المصنوعة من المواد البلاستيكية فإن موجات التذبذب في الضغط تتشتت بسرعة ويزداد طولها الموجي. هذا التأثير ناتج عن التأخر فى حدوث التغير فى شكل جدران الأنبوب. يقدم هذا البحث نموذجاً رياضياً لمحاكاة ظاهرة الطرق المائي في الأنابيب المصنوعة من المواد البلاستيكية. يعتمد هذا النموذج الرياضي على استخدام "نموذج كلفن-فويت" (Kelvin–Voigt model) لتوصيف السلوك الميكانيكي لجدران الأنابيب المصنوعة من البلاستيك. وقد تم حل المعادلات بالنموذج المقدم بطريقة الصفات المميزة (Method of Characteristics) ، مع إهمال كل من تأثير التفاعل بين السائل والبنية (fluid-structure interaction) وتأثير الاحتكاك غير المستقر (unsteady friction). تم أيضاً مقارنة النتائج النظرية لهذا النموذج بالنتائج العملية لأحد المراجع. كما تمت دراسة تأثير كل من الخطوة الزمنية وكذا سرعة الموجة على شكل موجة التذبذب في الضغط. وقد خلصت الدراسة إلى أن السلوك الميكانيكي لجدران الأنابيب المصنوعة من البلاستيك له التأثير الأكبر على شكل موجة الضغط المتولدة أثناء حدوث ظاهرة الطرق المائي. كما وجد أن الخطوة الزمنية تؤثر على كل من قيمة الذروة وكذا التردد للموجة بينما تؤثر سرعة الموجة على التردد فقط ؛ حيث نجد أن أفضل نتائج يمكن الحصول عليها عند رقم كورنت (Courant number) يتراوح ما بين 0.983 إلى الوحدة وعندما تكون سرعة الموجة حوالى 388.7 م/ث ؛ حيث يكون عندها متوسط كلاً من السعة والتردد لموجات التذبذب في الضغط للحل العددي هما 96% و 95.1% من القيم المناظرة للنتائج العملية ، على الترتيب.

ABSTRACT

The mechanical behavior of the pipe material affects the pressure response of a fluid system during water hammer. In viscoelastic pipes, the pressure fluctuations are rapidly attenuated and the pressure wave is delayed in time. This is due to the retarded deformation of the pipe-wall. In this work, a mathematical model to simulate water hammer in viscoelastic pipes taking into account the viscoelastic behavior of pipe walls, applying the Kelvin–Voigt model, has been developed. The developed model was solved using the Method of Characteristics (MOC), neglecting fluid-structure interactions (FSI) and unsteady friction effects. The model results were tested against the experimental results obtained by Covas et al. [1], which carried out on a high density polyethylene (HDPE) pipe-rig at Imperial College, London. The effects of time step and wave speed were studied. The pressure fluctuation obtained with the proposed viscoelastic model showed a good agreement with the experimental results. Conversely, the pressure obtained by the elastic model solution showed a large discrepancy with the experimental and numerical data. The time step affected the pressure-head wave amplitude and frequency, while wave speed affected only the wave frequency. The best results were obtained at higher time step values, corresponding to a Courant number ranging from 0.983 to unity, as the average amplitude and frequency of the numerical solution are 96% and 95.1% of their corresponding values for the experimental results, respectively. The best wave speed was at about 388.7 m/s.

Keywords: Water Hammer – Viscoelasticity – Methods of Characteristics – Courant Number – Wave Speed

1. INTRODUCTION

In recent years, the application of plastic pipes, such as polyethylene (PE), polyvinyl chloride (PVC) and polypropylene (PP) have been increasingly used in water supply systems due to their high mechanical, chemical and temperature

Accepted September 30, 2013

resistant properties, light weight and easy and fast installation. Hydraulic transient in pipes is important for the design of water pipeline systems. Analysis of transient flow helps in selecting pipe materials, pressure classes and specifying of surge protection devices to withstand additional loads resulting from water hammer phenomenon.

Classic water hammer theory based on the assumptions of linear elastic behavior of pipe walls and quasi-steady-state friction losses (Chaudhry [2], Wylie and Streeter [3,4]). This approach is relatively accurate to predict hydraulic transients in metal or concrete pipes, but for plastic pipes it is considerably imprecise. This is because polymers, in general, exhibit a viscoelastic mechanical behavior (Ferry [5], Riande et al. [6]) which influences the pressure response of the pipe system during transient events. The viscoelastic behavior attenuates the pressure fluctuations rapidly, delays the pressure wave in time and increases the dispersion of the travelling wave. This effect has been experimentally observed by several researchers (Covas et al. [1], Fox and Stepnewski [7], MeiBner and Franke [8], Williams [9], Mitosek and Roszkowski [10], Brunone et al. [11], Kodura and Weinerowska [12], Bergant et al. [13] and Bergant et al. [14]). Many other authors proposed mathematical models to simulate fluid transients in viscoelastic pipes taking viscoelasticity of pipe-wall into account (Bergant et al. [14], Gally et al. [15], Rieutford and Blanchard [16], Rieutford [17], Franke and Seyler [18], Suo and Wylie [19], Covas [20], Covas et al. [21], Duan [22], Bergant et al. [23] and Keramat et al. [24]).

Although viscoelasticity has a significant effect on simulation of fluid transients in viscoelastic pipes, FSI and unsteady friction affect also simulation results. FSI effect was investigated by many authors (Keramat et al. [24], Lavooij and Tijsseling [25], Tijsseling [26], Heinsbroek [27], Wiggert and Tijsseling [28], Neuhaus and Dudlik [29] and Achouyab and Bahrar [30]). They found that the FSI has no significant effect if the pipe was fixed rigidly and constrained from any axial movement.

Several researchers took the effect of unsteady friction into account while simulating fluid transients in viscoelastic pipes (Duan [22], Zielke [31], Brunone et al. [32], Bergant et al. [33], Ghidaoui et al. [34], Adamkowski and Lewandowski [35], Pezzinga [36], Brunone and Berni [37] and Storli and Nielsen [38]). They found that the viscoelastic effect becomes more and more dominant with respect to unsteady friction, as time progresses (Meniconi et al. [39]).

In this paper, a mathematical model which simulates water hammer in viscoelastic pipes was developed and solved using the MOC. In the proposed model, only viscoelasticity was taken into account, neglecting FSI and unsteady friction effects. Viscoelasticity was simulated applying a generalized Kelvin–Voigt model. The model was verified by comparing the model numerical results with the experimental results observed by Covas et al. [1].

2. MATHEMATICAL MODEL

2.1. Viscoelasticity

Viscoelastic materials exhibit both viscous and elastic characteristics when undergoing deformation due to its molecular nature. When viscoelastic materials subjected to a certain instantaneous stress σ_0, they do not respond according to Hooke's law. The viscosity of the viscoelastic material gives the substance a strain rate which is dependent on time. These materials have an instantaneous elastic response and a retarded viscous response, as shown in Fig. 1(a), so that the total strain ε can be decomposed into an instantaneous-elastic strain, ε_e, and a retarded strain, ε_r as:

$$\varepsilon = \varepsilon_e + \varepsilon_r(t) \tag{1}$$

For small strains, applying "Boltzmann superposition principle", a

combination of stresses that act independently results in strains that can be added linearly. This is shown in Fig. 1(b) for the particular case of two stresses. So, the total strain generated by a continuous application of stress $\sigma(t)$ is (Bergant et al. [23]):

$$\varepsilon = \sigma(t)\, J_0 + \left(\sigma(t) * \frac{\partial J(t)}{\partial t} \right) \qquad (2)$$

where J_0 is the instantaneous creep-compliance and "*" denotes convolution. For linearly elastic materials, the constant creep-compliance J_0 is equal to the inverse of Young's modulus of elasticity, i.e., $J_0 = 1/E_0$.

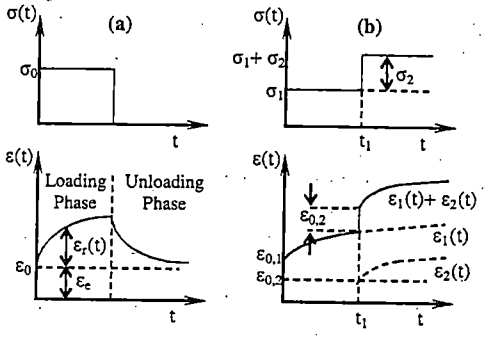

Figure 1 (a) Stress and strain for an instantaneous constant load (b) Boltzmann superposition principle for two stresses applied sequentially

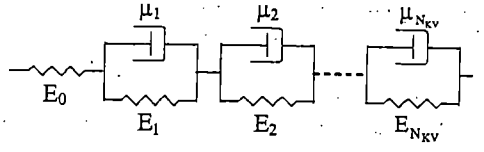

Figure 2 Generalized Kelvin–Voigt model

In order to determine stress-strain interactions and temporal dependencies of viscoelastic materials, many viscoelastic models have been developed. For small deformations, it is usually applicable to apply linear viscoelastic models, for example a generalized Kelvin–Voigt model consisting of N_{KV} parallel spring and dashpot elements in series with one additional spring, as shown in Fig. 2. In this mechanical model, the elastic behavior of viscoelastic materials is modeled using springs, while dashpots are used to model the viscous behavior. It is used to describe the creep function (Aklonis et al. [40]) as follows:

$$J(t) = J_0 + \sum_{k=1}^{N_{KV}} J_k \left(1 - e^{-t/\tau_k}\right) \qquad (3)$$

where J_k is defined by $J_k = 1/E_k$, J_k and E_k are the creep-compliance and the modulus of elasticity of the spring of the Kelvin–Voigt k-element, and $\tau_k = \mu_k/E_k$. τ_k and μ_k are the retardation time and the viscosity of the dashpots of k-element. The parameters J_k and τ_k of the viscoelastic mechanical model are adjusted to the creep-compliance experimental data. The creep-compliance function for a material is dependent on temperature, stress, age, and orientation as a result of the manufacturing process (Lai and Bakker [41]). These effects are not included in Eq. (3).

The total strain indicated by Eq. (2) consists of an elastic and a viscoelastic part. The viscoelastic part is a function of the whole loading history. In the case of water hammer, this loading comes from the fluid pressure head within the pipe. The steady head H_0 accounts for the static situation as one can assume that a long time has been passed after the establishment of H_0. The dynamic head $\overline{H}$ represents the difference between the fluid pressure head H and static head H_0 as follows:

$$\overline{H} = H - H_0 \qquad (4)$$

If the dynamic head is substituted for stress σ in the integrand of Eq. (2), a function which represents up to a constant factor the retarded response to water hammer is given by (Keramat et al. [24]):

$$I_{\overline{H}}(t) = \sum_{k=1}^{N_{KV}} \left(\frac{J_k}{\tau_k} \int_0^t \overline{H}(t-s) e^{-s/\tau_k} ds \right) = \sum_{k=1}^{N_{KV}} I_{\overline{H}k}(t) \qquad (5)$$

2.2. Governing Equations

In this section, the governing equations for water hammer in a viscoelastic pipe are presented (Keramat et al. [24]). In the presented model, the relevant assumptions are: the piping system consists of thin-walled, linearly viscoelastic pipes with no buckling and no large deformations and neglecting fluid-structure interactions (FSI), unsteady friction and convective terms. Another important assumption made in this derivation is that the pipe is totally restrained from axial movements. Applying the Kelvin-Voigt model to simulate viscoelasticity, then the continuity and momentum equations can be written in the following forms:

$$\frac{\partial V}{\partial s}+\frac{g}{a^2}\frac{\partial H}{\partial t}+2\frac{\partial \varepsilon_\varphi}{\partial t}=0 \qquad (6)$$

$$\frac{\partial V}{\partial t}+\frac{1}{\rho}\frac{\partial p}{\partial s}+g\frac{dz}{ds}+\frac{f}{2D}V|V|=0 \qquad (7)$$

where,

$$\varepsilon_\varphi=\left(1-\nu^2\right)\left(\sigma_\varphi * dJ\right) \qquad (8)$$

The thin-walled pipe assumption also allows the dynamic circumferential hoop stress to be calculated according to:

$$\sigma_\varphi=\frac{\rho g D\overline{H}}{2e} \qquad (9)$$

Using Eqs. (8) and (9) in (6), and eliminating the convolution operator, Eq. (6) can be rewritten in the pressure form as follows:

$$a^2\frac{\partial V}{\partial s}+\frac{1}{\rho}\left(\frac{\partial p}{\partial t}\right)+C_{01}=0 \qquad (10)$$

where

$$C_{01}=\left[\left(g\frac{\partial s}{\partial t}\frac{\partial z}{\partial s}\right)+a^2\left(1-\nu^2\right)\frac{\rho g D}{e}\frac{\partial I_{\overline{H}}}{\partial t}\right]$$

2.3. MOC Implementation

From the previous section, the continuity and momentum equations, which govern unsteady fluid flow in pipelines, are found as partial differential equations. The standard procedure to solve these equations is the method of characteristics (MOC). This procedure yields water-hammer compatibility equations that are valid along characteristic lines in the distance (s)–time (t) plane.

2.3.1 Development of the characteristic equations

Multiplying Eq. (7) by Lagrange multiplier, a constant linear scale factor (λ), and adding the result to Eq. (10), get:

$$\left(\lambda\frac{\partial V}{\partial t}+a^2\frac{\partial V}{\partial s}\right)+\left(\frac{1}{\rho}\frac{\partial p}{\partial t}+\frac{\lambda}{\rho}\frac{\partial p}{\partial s}\right)+g\lambda\frac{dz}{ds}+\frac{f\lambda}{2D}V|V|+C_{01}=0 \qquad (11)$$

The first group can be replaced by $\lambda\cdot dV/dt$, then $a^2=\lambda\cdot ds/dt$, while the second group can be replaced by $1/\rho\cdot dp/dt$, then $\lambda=ds/dt$. To satisfy these two requirements for ds/dt, then $\lambda^2=a^2$. This leads to:

$$\lambda=\pm a \qquad (12)$$

Then Eq. (11) after replacing groups can be rewritten as follows:

$$\left(\lambda\frac{dV}{dt}\right)+\left(\frac{1}{\rho}\frac{dp}{dt}\right)+g\lambda\frac{dz}{ds}+\frac{f\lambda}{2D}V|V|+C_{01}=0 \qquad (13)$$

Replacing Lagrange multiplier with its values from Eq. (12), then Eq. (13) can be rewritten in the head form, as it is easier to visualize the propagation of pressure waves, as follows:

$$\frac{dV}{dt}\pm\frac{g}{a}\left(\frac{dH}{dt}\right)+\frac{f}{2D}V|V|\pm\frac{C_{01}}{a}=0$$

$$\text{only when}\left[\frac{ds}{dt}=\pm a\right] \qquad (14)$$

Eq. (14) represents the characteristic equations. These equations describe a family of straight lines of slope ($\pm 1/a$) on the *s-t* plan. Figure 3 shows the C^+ and C^- characteristic lines on the *s-t* plane for a reservoir-pipe-valve system.

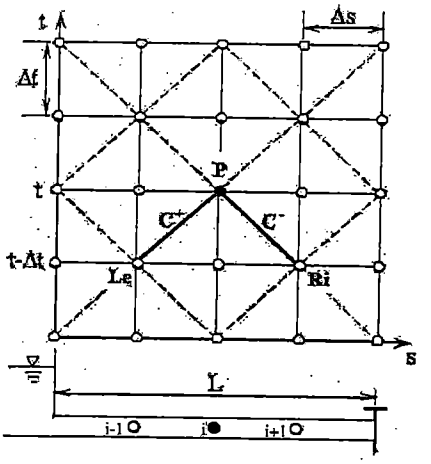

Figure 3 The MOC grid for a reservoir-pipe-valve system

2.3.2 *The finite difference equations representation*

In order to get the numerical solution of Eq. (14), they have to be written in finite difference form. It will become:

$$(V_p-V_{Le})+\frac{g}{a}(H_p-H_{Le})+\frac{f\Delta t}{2D}V_{Le}|V_{Le}|+\frac{C_{01}\Delta t}{a}=0 \qquad (15)$$

$$(V_p-V_{Ri})-\frac{g}{a}(H_p-H_{Ri})+\frac{f\Delta t}{2D}V_{Ri}|V_{Ri}|-\frac{C_{01}\Delta t}{a}=0 \qquad (16)$$

The term $\left[\frac{C_{01}\Delta t}{a}\right]$ can be rewritten in the following form:

$$\frac{C_{01}\Delta t}{a}=\left[\pm\left(g\Delta t\frac{\partial z}{\partial s}\right)+C_{07}\left(\frac{\partial I_{\overline{H}}}{\partial t}\right)\right]$$

$$\text{only when}\left[\frac{ds}{dt}=\pm a\right] \qquad (17)$$

where, $C_{07}=(1-\nu^2)\Delta t.a\frac{\rho gD}{e}$.

By substitution in Eqs. (15) and (16), get:

$$(V_p-V_{Le})+\frac{g}{a}(H_p-H_{Le})+\frac{f\Delta t}{2D}V_{Le}|V_{Le}|+(g\Delta t.\sin\theta)+C_{07}\left(\frac{\partial I_{\overline{H}}}{\partial t}\right)=0 \qquad (18)$$

$$(V_p-V_{Ri})-\frac{g}{a}(H_p-H_{Ri})+\frac{f\Delta t}{2D}V_{Ri}|V_{Ri}|+(g\Delta t.\sin\theta)-C_{07}\left(\frac{\partial I_{\overline{H}}}{\partial t}\right)=0 \qquad (19)$$

where $\sin\theta = (\partial z/\partial s)$ is positive for pipes sloping upward in the downstream direction. Keramat et al. [24] evaluated the term $(\partial I_{\overline{H}}/\partial t)$ using the following linear relation for the unknown head at the current time step:

$$\frac{\partial I_{\overline{H}}}{\partial t}=\sum_{k=1}^{N_{KV}}\frac{\partial I_{\overline{H}k}}{\partial t}=a_1H_p(t)+a_2 \qquad (20)$$

where,

$$a_1=\sum_{k=1}^{N_{KV}}\left[\frac{J_k}{\Delta t}\left(1-e^{\frac{\Delta t}{\tau_k}}\right)\right]\equiv Sum_{01} \qquad (21)$$

$$a_2=a_3\left[H_p(t-\Delta t)-H_0\right]-a_1\left[H_p(t-\Delta t)\right]-a_4 \qquad (22)$$

$$a_3=\sum_{k=1}^{N_{KV}}\left[\frac{J_k}{\tau_k}\left(e^{\frac{\Delta t}{\tau_k}}\right)\right]\equiv Sum_{02} \qquad (23)$$

$$a_4=\sum_{k=1}^{N_{KV}}\left[\frac{e^{\frac{\Delta t}{\tau_k}}}{\tau_k}I_{\overline{H}k}(t-\Delta t)\right]\equiv Sum_{03} \qquad (24)$$

Then, Eqs. (18) and (19) can be rewritten as follows:

$$(V_p - V_{Le}) + \left(\frac{g}{a} + C_{08}\right) H_p - \left(\frac{g}{a}\right) H_{Le} + \frac{f\Delta t}{2D} V_{Le} \mid V_{Le} \mid + (g\Delta t . \sin\theta) + C_{09} = 0 \quad (25)$$

$$(V_p - V_{Ri}) - \left(\frac{g}{a} + C_{08}\right) H_p + \left(\frac{g}{a}\right) H_{Ri} + \frac{f\Delta t}{2D} V_{Ri} \mid V_{Ri} \mid + (g\Delta t . \sin\theta) - C_{09} = 0 \quad (26)$$

where $C_{08} = (C_{07} * a_1)$ and $C_{09} = (C_{07} * a_2)$.

Equations (25) and (26) represent the C^+ and C^- characteristic lines equations.

3. MODEL VERIFICATION

To verify the proposed mathematical model and its solutions, a case study presented experimentally by Covas et al. [1] was investigated.

Covas et al. [1] performed an experiment on a high density polyethylene (HDPE) pipe-rig, which is rigidly fixed to a wall with the specifications given in Table 1. It is a reservoir-pipeline-valve system where the length between the vessel and the downstream globe valve is 277 m.

Covas et al. [21] performed creep tests to determine the creep function of HDPE. They also estimated the order of magnitude of this creep function based on data collected from the pipe-rig and in the calibration of a mathematical model developed by Covas et al. [1]. The creep function provided by Covas et al. [21] is used (Table 2).

The developed mathematical model results for the heads at location 5, corresponding to a distance of 197 m from the upstream end are compared with the experimental results of Covas et al. [1] in Figure 4.

It can be observed that viscoelasticity has been modelled and implemented herein correctly, The effect of FSI was not significant in the experimental results because the test-rig pipe sections were rigidly fixed and assumed to be constrained from any axial movement.

Table 1. Specifications of the reservoir-pipeline-valve experiment performed by Covas et al. [1]

Length	277 m
Inner diameter	50.6 mm
Wall thickness	6.3 mm
Poisson ratio	0.46
Steady state discharge	1.01 l/s
Reservoir head	45 m
Valve closure time	0.09 s
Pressure wave speed	385.0 m/s
Stress wave speed	630.0 m/s

Table 2. Calibrated creep coefficients J_k Covas et al. [21]

Sample size	20 s	
Number of K-V elements	5	
Retardation times τ_k (s) and creep coefficients J_k (10^{-10} Pa^{-1})	$\tau_1 = 0.05$	$J_1 = 1.057$
	$\tau_2 = 0.50$	$J_2 = 1.054$
	$\tau_3 = 1.50$	$J_3 = 0.9051$
	$\tau_4 = 5.0$	$J_4 = 0.2617$
	$\tau_5 = 10.0$	$J_5 = 0.7456$

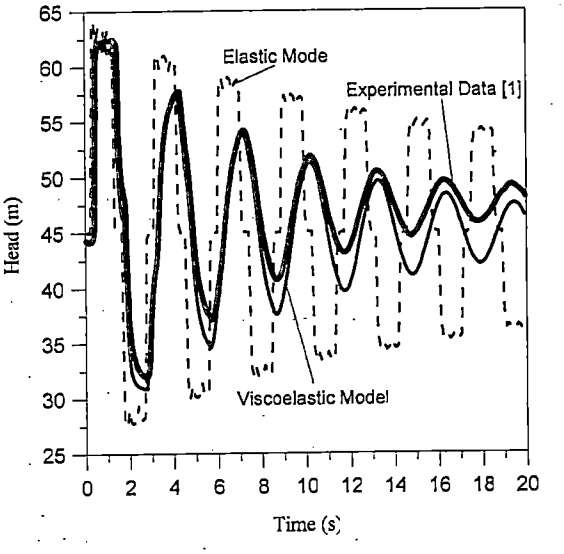

Figure 4 Comparison of the mathematical model results against the experimental results of Covas et al. [1] at location (5)

The viscoelastic effect becomes more dominant with respect to unsteady friction, as time progresses. So, acceptable discrepancy between the numerical and experimental results with time progress can be observed, due to neglecting the unsteady

friction effect in the present model. For the viscoelastic model, the figure also shows that the pressure wave damps faster than damping in the elastic model, which agrees with the experimental results. Therefore, in case of studying viscoelastic pipes the viscoelastic model should be applied to predict pressure head fluctuations.

4. PARAMETERS AFFECTING VISCOELASTIC MODEL

From Eqs. (25) and (26), it is clear that the time step, Δt, and the wave speed, a, appear in more than one term. Therefore, these parameters may lead to a significant effect on viscoelastic results. Therefore, their effect on the viscoelastic model results will be investigated herein.

4.1 Time Step Effect

In this section, the time step effect on the viscoelastic model is investigated by varying the time step value. The stability criterion for explicit time stepping developed by Courant et al. [42] must be satisfied. This criterion requires that the Courant number, C, which is defined by Eq. (27), must not exceed the unity.

$$C = \frac{\Delta t \times max|a+V|}{\Delta s} \leq 1 \qquad (27)$$

Therefore, the time step value can be changed within the following limit:

$$\Delta t \leq \frac{\Delta s}{max|a+V|} \qquad (28)$$

For a wave speed of 385 m/s, the effect of varying the time step and consequently Courant number values is shown in Figure 5. It reveals that changing time step and Courant number causes amplitude and frequency distortions. The amplitude distortion is illustrated in Figure 6, whereas the frequency distortion is shown in Figure 7.

Figure 6 represents a comparison between the average head of Covas et al. [1] data and those of the numerical results at different time steps. The average head ratio is the ratio of the numerical results average head to their corresponding values of the experimental data obtained by Covas et al. [1] at different time steps. It shows that the average amplitude of the numerical solution at Courant number of 1 is 96 % of its value for the experimental results.

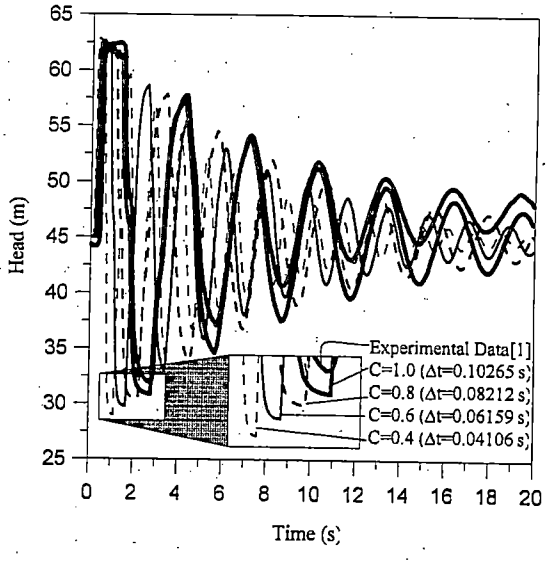

Figure 5 Time-step and Courant number effects on head fluctuations

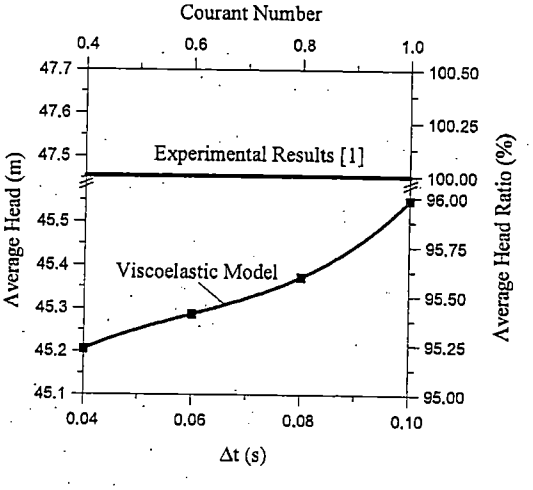

Figure 6 Time step and Courant number effects on average head value

Figure 7 represents a comparison between the frequency of fluctuating head of Covas et al. [1] data and those of the numerical results at different time steps. The average frequency ratio is the ratio of

the numerical results average frequency to their corresponding values of the experimental data obtained by Covas et al. [1] at different time steps. It shows that the average frequency of the numerical solution at Courant number of 1 is 95.1 % of its value for the experimental results.

From Figures 6 and 7, it is clear that the higher time step and Courant number gives the best match. The best amplitude match can be obtained at Courant number equals unity, while the best frequency match is achieved at Courant number of 0.983. At this Courant number, the amplitude distortion will be quiet large. While at Courant number equals to unity, the frequency distortion will be quiet small. So, it is recommended to choose Courant number equals to unity to get the optimum match.

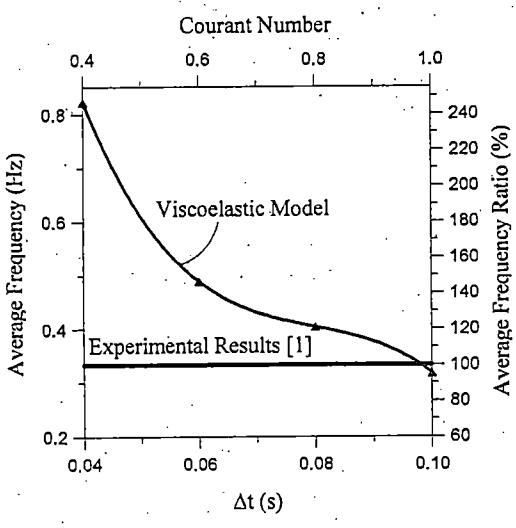

Figure 7 Time step and Courant number effects on average frequency of fluctuating head

4.2 Wave Speed Effect

Wave speed for a pipe anchored throughout against axial movement was presented by Larock et al. [43] as follows:

$$a = \sqrt{\frac{K/\rho}{1+\left[\left(\frac{K}{E}\right)\left(\frac{D}{e}\right)\left(1-\upsilon^2\right)\right]}} \qquad (29)$$

While the HDPE modulus of elasticity varies from 0.8 to 1.43 GPa [44,45], then the wave speed value can vary from 345 m/s to 452 m/s, respectively. Figure 8 illustrates the effect of wave speed change within the previous range at Courant number of unity.

Figure 8 shows that changing wave speed has no significant effect on pressure-head wave amplitude, while it affects the wave frequency.

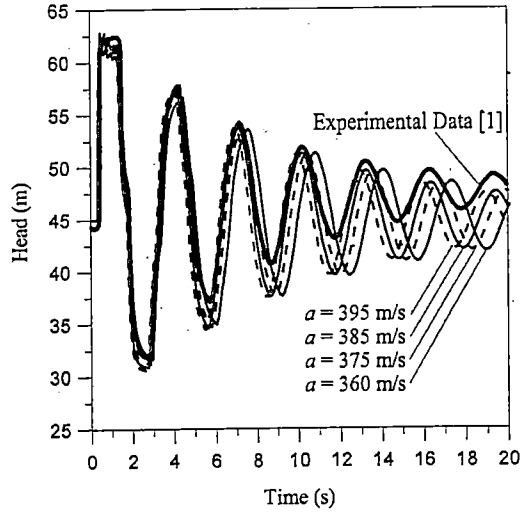

Figure 8 Wave speed effect on head fluctuations

For a certain wave speed, it can be observed that the wave frequency changes with time. This effect can be observed from Figure 9. It shows the change in wave frequency as a function of time and the comparison with experimental results.

From Figure 9, it is clear that for all wave speeds the pressure-head wave frequency decreases with time, while for the experimental results it tends to decrease firstly and there is a slight increase when time progress.

Figure 10 represents the relation between average pressure-head wave frequency as a function of wave speed. It shows that the higher wave speed, the higher average pressure-head wave frequency.

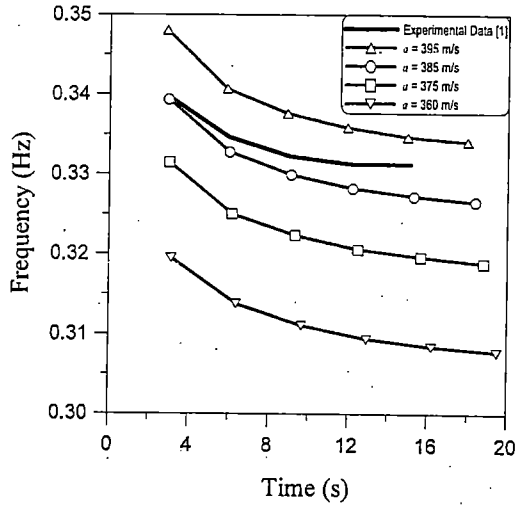

Figure 9 Wave speed effect on wave frequency

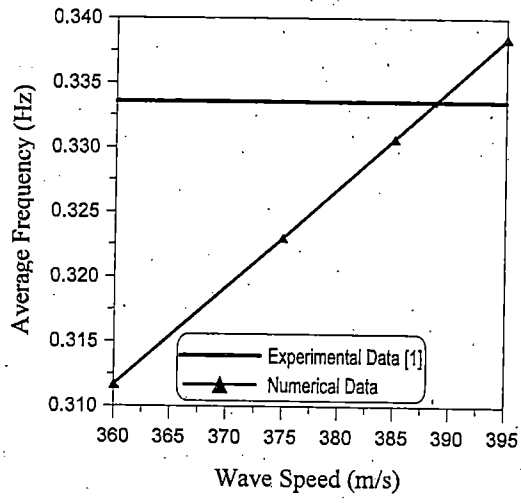

Figure 10 Wave speed effect on average wave frequency

5. CONCLUSIONS

A mathematical model to calculate water hammer in viscoelastic pipes taking into account the viscoelastic behavior of pipe walls has been developed in the current paper. Viscoelastic behavior was simulated by applying the Kelvin-Voigt model. Governing equations for water hammer in a viscoelastic pipe were solved using MOC neglecting FSI and unsteady friction. To verify the proposed mathematical model and its numerical implementation, its results were compared with the experimental data. The numerical results obtained by the elastic and the viscoelastic models were compared with experimental results carried out on a HDPE pipe-rig by Covas et al. [1]. The effects of time-step, Courant number and wave speed were studied.

The pressure fluctuation obtained with the proposed viscoelastic model agreed, within 96%, with the experimental data. Conversely, the pressure obtained by the elastic model solution showed a large discrepancy with the experimental and theoretical data. So, taking viscoelasticity into account was very important while simulating transient events in a viscoelastic pipe. However, neglecting FSI in the current model did not affect the results significantly, as the test rig pipe sections were rigidly fixed and assumed to be constrained from any axial movement. On other hand, neglecting the unsteady friction affected the model results slightly with time.

The time step and Courant number affects the pressure-head wave amplitude and frequency. The higher time step and Courant number, the best match between the numerical and experimental results. Best results can be obtained at a Courant number ranging from 0.983 to unity.

Wave speed affects the pressure-head wave frequency, as increasing wave speed increases the average pressure-head wave frequency. The deviation between the numerical and experimental results may be due to the wave speed value, a, which depends on the fixation type and the value of the modulus of elasticity that varies from 0.8 to 1.43 GPa.

NOMENCLATURE

a	Wave speed, m/s
C	Courant number
D	Pipe internal diameter, m
e	Pipe wall thickness, m
E	Pipe modulus of elasticity, Pa
f	Friction coefficient
g	Gravitational acceleration, m/s^2

H	Head, m
H_0	Head at steady state condition, m
$\overline{H}$	Dynamic head (H–H_0), m
H_{sump}	Sump level, m
h_P	Head increase across a pump, m
$I_{\overline{H}}$	a function representing the retarded response to water hammer
J	Creep compliance function, Pa^{-1}
K	Fluid bulk modulus, Pa
L	Pipe length, m
N_{KV}	Number of Kelvin-Voigt elements
p	Pressure, Pa
Q	Discharge, m^3/s
Q_P	Discharge of a pump, m^3/s
s	Axial coordinate
t	Time, s
t_c	Valve closure time, s
V	Fluid velocity, m/s
V_0	Fluid velocity at steady state condition, m/s
z	Elevation, m
Δ	Difference
ε	Strain
ε_φ	Circumferential strain
θ	Pipe inclination angle, degree
λ	Lagrange multiplier
υ	Poisson's ratio
ρ	Fluid density, kg/m^3
σ_φ	Circumferential stress, Pa
τ	Retardation time, s

REFERENCES

[1] Covas, D., Stoianov, I., Mano, J., Ramos, H., Graham, N. and Maksimovic, C., The dynamic effect of pipe-wall viscoelasticity in hydraulic transients. Part I—experimental analysis and creep characterization, *Journal of Hydraulic Research*, Vol. 42, pp. 516–530, 2004.

[2] Chaudhry, M. H., *Applied Hydraulic Transients*, 2nd edition, Litton Educational Publishing Inc., Van Nostrand Reinhold Co., New York, 1987.

[3] Wylie, E. B. and Streeter, V. L., *Fluid Transients*, Thomson-Shore, Dexter, 1988.

[4] Wylie, E. B. and Streeter, V. L., *Fluid Transients in Systems*, Prentice Hall, Englewood, 1993.

[5] Ferry, J. D., *Viscoelastic Properties of Polymers*, 2nd edition, John Wiley & Sons, New York, 1970.

[6] Riande, E., Díaz-Calleja, R., Prolongo, M., Masegosa, R. and Salom, C., *Polymer Viscoelasticity: Stress and Strain in Practice*, Marcel Dekker, Inc., New York, 2000.

[7] Fox, J., and Stepnewski, D., Pressure wave transmission in a fluid contained in a plastically deforming pipe, *Journal of Pressure Vessel Technology*, Transactions of the ASME, pp. 258–262, 1974.

[8] MeiBner, E. and Franke, G., Influence of pipe material on the dampening of waterhammer, Proceedings of the 17th Congress of the International Association for Hydraulic Research, IAHR, Baden-Baden, Germany, 1977.

[9] Williams, D., Waterhammer in non-rigid pipes: precursor waves and mechanical dampening, *Journal of Mechanical Engineering*, ASME, Vol. 19, pp. 237–242, 1977.

[10] Mitosek, M. and Roszkowski, A., Empirical study of waterhammer in plastic pipes, *Plastics, Rubber Composites Process Applications*, Vol. 27, pp. 436–439, 1998.

[11] Brunone, B., Karney, B. W., Mecarelli, M. and Ferrante, M., Velocity profiles and unsteady pipe friction in transient flow, *Journal of Water Resources Planning and Management*, Vol. 126, pp. 236–244, 2000.

[12] Kodura, A. and Weinerowska K., The influence of the local pipe leak on the properties of the water hammer, Proceedings of the 2nd Congress of Environmental

Engineering, Lublin, Poland, Vol. 1, pp. 399–407, 2005.

[13] Bergant, A., Tijsseling, A., Vitkovsky, J., Covas, D., Simpson, A. and Lambert, M., Parameters affecting water-hammer wave attenuation, shape and timing—Part 2: Case studies, *Journal of Hydraulic Research*, Vol. 46, pp. 382–391, 2008.

[14] Bergant, A., Hou, Q., Keramat, A. and Tijsseling, A., Experimental and numerical analysis of water hammer in a large-scale PVC pipeline apparatus, Report 11-51, Department of Mathematics and Computer Science, Eindhoven University of Technology, Eindhoven, The Netherlands, 2011.

[15] Gally, M., Guney, M. and Rieutford, E., An investigation of pressure transients in viscoelastic pipes, *Journal of Fluids Engineering*, Transactions of the ASME, Vol. 101, pp. 495–499, 1979.

[16] Rieutford, E. and Blanchard, A., Ecoulement non-permanent en conduite viscoelastique–coup de belier, *Journal of Hydraulic Research*, IAHR, Vol. 17, pp. 217–229, 1979.

[17] Rieutford, E., Transients response of fluid viscoelastic lines, *Journal of Fluids Engineering*, ASME, Vol. 104, pp. 335–341, 1982.

[18] Franke, G. and Seyler, F., Computation of unsteady pipe flow with respect to viscoelastic material properties, *Journal of Hydraulic Research*, IAHR, Vol. 21, pp. 345–353, 1983.

[19] Suo, L. and Wylie, E., Complex wave speed and hydraulic transients in viscoelastic pipes, *Journal of Fluids Engineering*, Transactions of the ASME, Vol. 112, pp. 496–500, 1990.

[20] Covas, D., Inverse transient analysis for leak detection and calibration of water pipe systems—modelling special dynamic effects, PhD Thesis, Imperial College of Science, Technology and Medicine, University of London, London, UK, 2003.

[21] Covas, D., Stoianov, I., Mano, J., Ramos, H., Graham, N. and Maksimovic, C., The dynamic effect of pipe-wall viscoelasticity in hydraulic transients. Part II— model development, calibration and verification, *Journal of Hydraulic Research*, Vol. 43, pp. 56–70, 2005.

[22] Duan, H.F., Relative importance of unsteady friction and viscoelasticity in pipe fluid transients, 33rd IAHR Congress: Water Engineering for a Sustainable Environment, Vancouver, British Columbia, Canada, 2009.

[23] Bergant, A., Tijsseling, A., Vitkovsky, J., Covas, D., Simpson, A. and Lambert, M., Parameters affecting water-hammer wave attenuation, shape and timing—Part 1: Mathematical tools, *Journal of Hydraulic Research*, Vol. 46, pp. 373–381, 2008.

[24] Keramat, A., Tijsseling, A. and Ahmadi, A., Investigation of transient cavitating flow in viscoelastic pipes, Report 10-39, Department of Mathematics and Computer Science, Eindhoven University of Technology, Eindhoven, The Netherlands, 2010.

[25] Lavooij, C. and Tijsseling, A., Fluid-structure interaction in liquid-filled piping systems, *Journal of Fluids and Structures*, Vol. 5, pp. 573–595, 1991.

[26] Tijsseling, A., Fluid-structure interaction in liquid-filled pipe systems: a review, *Journal of Fluids and Structures*, Vol. 10, pp. 109–146, 1996.

[27] Heinsbroek, A., Fluid–structure interaction in non-rigid pipeline systems, *Nuclear Engineering and Design*, Vol. 172, pp. 123–135, 1997.

[28] Wiggert, D. and Tijsseling, A., Fluid transients and fluid-structure interaction in flexible liquid-filled piping, *Applied Mechanics Reviews*, Vol. 54, pp. 455–481, 2001.

[29] Neuhaus, T. and Dudlik, A., Experiments and comparing calculations on thermohydraulic pressure surges in pipes, *Kerntechnik*, Vol. 71, pp. 87–94, 2006.

[30] Achouyab, E. and Bahrar, B., Modeling of transient flow in plastic pipes, *Contemporary Engineering Sciences*, Vol. 6, pp. 35–47, 2013.

[31] Zielke, W., Frequency dependent friction in transient pipe flow, *Journal of Basic Engineering*, Vol. 90, pp. 109–115, 1968.

[32] Brunone, B., Golia, U. and Greco, M., Effects of two-dimensionality on pipe transients modeling, *Journal of Hydraulic Engineering*, Vol. 121, pp. 906–912, 1995.

[33] Bergant, A., Simpson, A. and Vitkovsky, J., Developments in unsteady pipe flow friction modelling, *Journal of Hydraulic Research*, Vol. 39, pp. 249–257, 2001.

[34] Ghidaoui, M., Zhao, M., McInnis, D., and Axworthy, D., A review of water hammer theory and practice, *Applied Mechanics Reviews*, Vol. 58, pp. 49–76, 2005.

[35] Adamkowski, A. and Lewandowski, M., Experimental examination of unsteady friction Models for transient pipe flow simulation, *Journal of Fluids Engineering*, Vol. 128, pp. 1351–1363, 2006.

[36] Pezzinga, G., Local balance unsteady friction model, *Journal of Hydraulic Engineering*, Vol. 135, pp. 45–56, 2009.

[37] Brunone, B. and Berni, A., Wall shear stress in transient turbulent pipe flow by local velocity measurement, *Journal of Hydraulic Engineering*, Vol. 136, pp. 716–726, 2010.

[38] Storli, P. and Nielsen, T., Transient friction in pressurized pipes. II: Two-coefficient instantaneous acceleration-based model, *Journal of Hydraulic Engineering*, Vol. 137, pp. 679–695, 2011.

[39] Meniconi, S., Brunone, B., Ferrante, M. and Massari, C., Numerical and experimental investigation of leaks in viscoelastic pressurized pipe flow, *Drinking Water Engineering and Science*, Vol. 6, pp. 11–16, 2013.

[40] Aklonis, J. J., MacKnight, W. J. and Shen, M., *Introduction to Polymer Viscoelasticity*, Wiley-Interscience, John Wiley & Sons, Inc., New York, 1972.

[41] Lai, J. and Bakker, A., Analysis of the non-linear creep of high-density polyethylene, *Polymer*, Vol. 36, pp. 93–99, 1995.

[42] Courant, R., Friedrichs, K. and Lewy, H., Über die partiellen Differenzengleichungen der mathematischen Physik, *Mathematische Annalen* (in German), Vol. 100, pp. 32–74, 1928.

[43] Larock, B., Jeppson, R. and Watters, G., *Hydraulics of Pipeline Systems*, CRC Press LLC, New York, 2000.

[44] Keramat, A., Tijsseling, A. and Ahmadi, A., Fluid-structure interaction with pipe-wall viscoelasticity during water hammer, Report 11-52, Department of Mathematics and Computer Science, Eindhoven University of Technology, Eindhoven, The Netherlands, 2011.

[45] http://www.engineeringtoolbox.com/young-modulus-d_417.html